**ACTA IMEKO**
**ISSN: 2221-870X**
*June 2025, Volume 14, Number 2, 1 - 8*

# Black-box modelling of electromagnetic compatibility in DC-DC converters for electric vehicles

**Ali Ait Salih[1], Zakaria M'barki[1], Youssef Mejdoub[1], Kaoutar Senhaji Rhazi[1]**

[1] *Laboratory of Networks, Computer Science, Telecommunication, Multimedia (RITM), CED Engineering Sciences, Higher School of Technology, Hassan II University, Casablanca, Morocco*

ABSTRACT
This paper aims to propose a generic black-box model for converters connected to an electric vehicle. The methodology for identifying the model parameters will be presented, as well as the validation of this model. In fact, the control of electromagnetic interference (EMI) in power converters for electric vehicles relies on several approaches, including soft switching and pseudo-random modulation, which aim to reduce voltage variations and spread EMI energy across a wide frequency band, respectively. However, filtering remains the most effective solution to mitigate common-mode and differential-mode noise while ensuring EMC compliance without compromising performance. Moreover, a black-box behavioural modelling approach in the frequency domain enables precise representation of EMI sources and the optimization of EMC filter design, focusing on common-mode and differential-mode impedances without requiring internal circuit details. Finally, a network-based modelling approach has been employed to define and compare theoretical impedances with experimental measurements, validating the EMC model by reconstructing the measured voltages and confirming its ability to accurately represent electromagnetic disturbances.

**Section:** RESEARCH PAPER

**Keywords:** Black box; DC-DC converter; conducted EMI; LISN; EMC

**Citation:** A. A. Salih, Z. M'barki, Y. Mejdoub, K. S. Rhazi, Black-box modelling of electromagnetic compatibility in DC-DC converters for electric vehicles, Acta IMEKO, vol. 14 (2025) no. 2, pp. 1-8. DOI: 10.21014/actaimeko.v14i2.2035

**Section Editor:** Luca Callegaro, INRiM, Italy

**Received** December 13, 2024; **In final form** March 8, 2025; **Published** June 2025



**Corresponding author:** Zakaria M'barki, e-mail: mbarki.ensem@gmail.com

## 1. INTRODUCTION

Power converters play a central role in the operation of electric vehicles (EVs) by ensuring efficient energy management and conversion between the various parts of the vehicle. EVs are equipped with propulsion systems powered by a high-voltage battery, but the various electronic and auxiliary components require different voltage levels to function properly. Converters, such as DC-DC converters and inverters, transform the energy from the main battery into the appropriate voltage for these components, including powering engine management systems, safety devices, lighting, and air conditioning. Additionally, power converters optimize the charging process for both the high-voltage battery and the auxiliary battery, thereby ensuring the vehicle's energy efficiency. Without these devices, it would be impossible to regulate energy distribution reliably and safely in an EV. Figure 1 provides a macroscopic overview of the range of power electronic converters used in electric vehicles (EVs), highlighting the critical functions of an onboard battery charger. These include interfacing with the three-phase AC power grid to enable AC/DC conversion, adapting the rectified voltage to match the onboard battery's voltage level via DC/DC conversion, ensuring high-quality current draw through Power

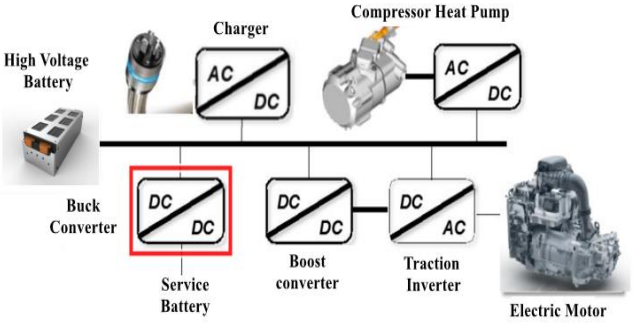


Figure 1. Example of an automotive electrical network and its main power electronic converters.

Factor Correction (PFC), and meeting Electromagnetic Compatibility (EMC) standards to prevent interference with other grid-connected devices and ensure user safety, which may involve EMC filtering and galvanic isolation depending on the chosen topologies. Our work in this article will be focused on the last function: EMC.

The integration of power electronic converters in electric vehicles requires strict management of RF emissions to ensure reliable operation. Electromagnetic compatibility (EMC) enables electronic systems to function effectively without generating or being affected by unwanted electromagnetic interference (EMI) [1], [2], [3]. This is crucial in electric vehicles, where the proximity of sensitive components and the need for high efficiency demand strict control of EMI.

Advancements in power electronics and the aim to reduce the mass and improve the efficiency of electrical energy distribution have led EV manufacturers to adopt high-voltage distribution systems, often operating at several hundred volts. As these operating voltages increase, the impact of the rate of voltage change (dV/dt) on conducted emissions becomes more significant. Higher dV/dt rates result from the fast-switching actions of power electronic devices[4], such as insulated gate bipolar transistors (IGBTs) or silicon carbide (SiC) MOSFETs, commonly used in onboard chargers, inverters, and DC-DC converters. These rapid transitions can induce high-frequency noise, leading to EMI issues that can affect the performance of both the vehicle's own systems and external devices. The environment of conducted EMI [5] in the onboard charging system of electric vehicles is illustrated in Figure 2.

Among the solutions considered for controlling EMI in electric vehicle power converters, several approaches stand out. Soft switching [6], [7], [8], [9] is one of them: it aims to reduce the rates of voltage and current variation during switching transitions, which significantly limits EMI generation. Another strategy is the use of pseudo-random modulation [10], [11], which spreads EMI energy across a wide frequency band, reducing emission peaks in specific ranges and minimizing interference risks. However, filtering remains the most effective solution. By incorporating EMC filters composed of inductors and capacitors, it is possible to attenuate common-mode and differential-mode noise [12], [13], ensuring EMC compliance without compromising system performance. Together, these strategies effectively reduce EMI while meeting the specific design requirements of electric vehicles.

Black-box [14] behavioural modelling in the frequency domain is a powerful method for accurately representing electromagnetic interference (EMI) sources in the design of electromagnetic compatibility (EMC) filters. It involves developing equivalent circuit models based on the system's common mode (CM) and differential mode (DM) impedance characteristics, as well as associated noise sources [15], [16]. Unlike analytical models, which require detailed knowledge of each system component, black-box modelling focuses on reproducing the overall behaviour of EMI sources without focusing on internal circuit details. CM and DM impedances are measured or simulated as a function of frequency to create a model that captures noise characteristics over a broad frequency range. This approach allows precise simulation and prediction of conducted EMI levels, facilitating the design and optimization of EMC filters that can reduce EMI emissions while preserving converter performance [17], [18]. It thus meets EMC regulatory requirements and minimizes the need for costly prototypes and testing in the final phase. It is in this context that we developed a "black box" model [19] to study EMI and assess the impact of the previously mentioned methods on emissions. Behavioural or "black box" modelling in the frequency domain allows precise representation of EMI sources in the design of EMC filters for electric vehicles. This approach relies on equivalent circuit models that enable the simulation and prediction of conducted EMI levels, thus facilitating emission reduction without compromising converter performance. By applying this method to a buck converter, it becomes possible to optimize filter components and their placement while adhering to the strict EMC standards of the automotive industry.

In this work, a network modelling of the equipment under test was performed to define an impedance matrix [20]. The theoretical impedances were calculated and compared to experimental measurements. The measured currents were corrected in MATLAB to improve accuracy, and the spectra of common-mode and differential-mode sources were calculated. Finally, the EMC model was validated by reconstructing and measuring the voltages across the LISN resistors, thus confirming its ability to accurately represent the electromagnetic disturbances.

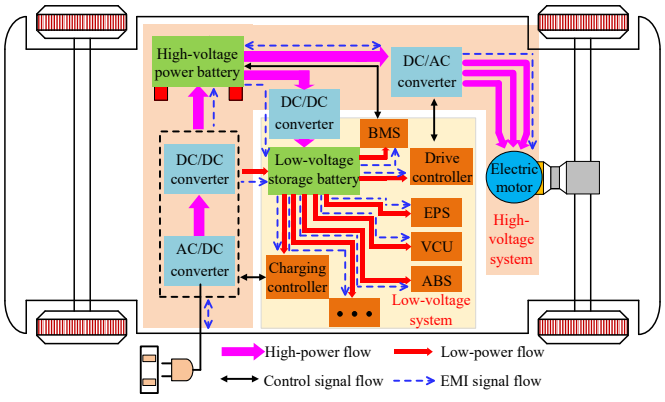


Figure 2. EMI environment in the onboard charging system.

## 2. ELECTROMAGNETIC MODELING OF A BUCK CONVERTER USED IN ELECTRIC VEHICLES

In this study, the choice was made to use a buck DC-DC converter [21], which is used to convert the 24 V battery voltage to a 12 V voltage to power the vehicle's auxiliary systems, such as lighting, the audio system, electric windows, etc. The converter under analysis includes an IRLZ44N MOSFET and a 1N5819 diode, operating in continuous conduction mode. Figure 3 shows the overall diagram of the studied system as implemented in the Matlab/Simulink environment [22], along with a simplified internal design of an open-loop Buck converter. The MOSFET is controlled by a PWM signal with a duty cycle D, which represents the percentage of time the MOSFET is on.

A low-pass filter, made up of an inductor and a capacitor, smooths the MOSFET's switching activity and provides a stable DC voltage. It is used to minimize the maximum current ripple in the inductor ($\Delta I_L = 10\ \%$) and the maximum voltage ripple across the load ($\Delta V_O = 4\ \%$). This Buck converter is designed to meet the requirements indicated in Table 1.

The system explored in this study consists of two access ports and a ground connection on the network side. Our goal is to characterize the parasitic behaviour of an existing converter from the perspective of the direct current (DC) network using an experimental approach, without any prior knowledge of its

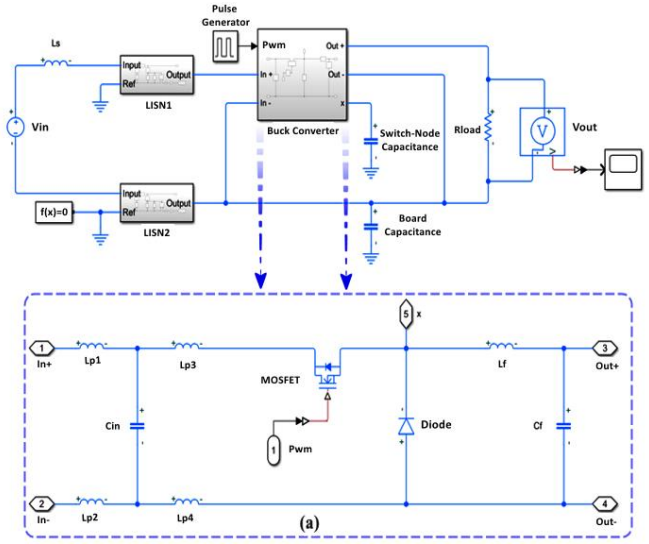


Figure 3. The entire system architecture with (a) The internal layout of the Buck converter's block.

Table 1. Simulation parameters.

| Parameter | Value |
|---|---|
| Input voltage $V_{in}$ | 24 V |
| Output voltage $V_O$ | 12 V |
| Load resistance $R_L$ | 24 Ω |
| Switching frequency $f_s = 1/T_s$ | 500 kHz |
| Inductance $L_F$ | 240 µH |
| Capacitance $C_F$ | 27 nF |
| Duty cycle *D* | 50 % |

internal electrical structure [23]. This electromagnetic compatibility model incorporates an IDM current source and a ZDM impedance between the two input lines to represent the differential mode. The common mode is depicted by two identical ZCM impedances connected to a VCM voltage source, placed between each line (a and b) and the ground (Figure 4).

By adopting a simplified measurement protocol that focuses on the separation of propagation modes, the identification of electromagnetic disturbance (EMC) sources in a DC/DC converter is significantly facilitated [24]. This approach effectively differentiates between differential mode and common mode disturbances, thereby enabling a more accurate characterization of the converter's parasitic effects. Once these disturbance modes are identified, the model supports the optimized design of filtering structures, each tailored to mitigate the respective common mode and differential mode disturbances.

The study examines a DC/DC converter that utilizes MOSFETs to power a resistive load designed to simulate the behaviour of an electrical lighting system, commonly found in electric vehicles. This configuration provides a realistic test environment for evaluating the EMC characteristics of the converter. The objective is to develop a robust strategy for mitigating EMC interference by addressing both common mode and differential mode disturbances, thereby enhancing the electromagnetic compatibility of the power system in electric vehicle applications [25].

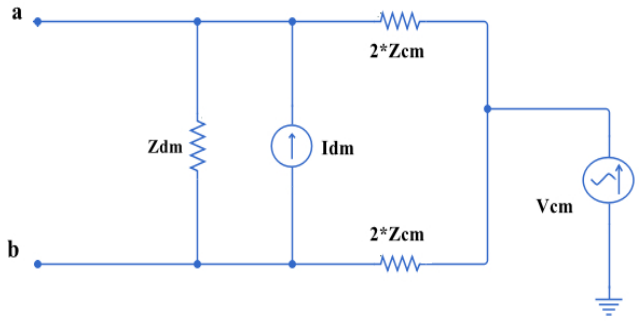


Figure 4. EMC model based on a "black-box" approach.

## 3. MODELING AND EXAMINING THE NETWORK-SIDE MODEL'S IMPEDANCE

The modelling of the equipment under test is approached from the network perspective, which includes two ports and a ground connection. As a result, the impedance matrix can be defined as follows:

$$[V] = [Z][I] \Rightarrow \begin{bmatrix} V_a \\ V_b \end{bmatrix} = \begin{bmatrix} Z_{aa} & Z_{ab} \\ Z_{ba} & Z_{bb} \end{bmatrix} \begin{bmatrix} I_a \\ I_b \end{bmatrix}. \quad (1)$$

The indices in equation (1) refer to the access letter shown in Figure 4. The common-mode and differential-mode quantities can be calculated based on the relations connecting the voltages and currents within the structure:

$$V_{DM} = V_a - V_b \; ; \; V_{CM} = \frac{V_a + V_b}{2} \quad (2)$$

$$I_{DM} = \frac{I_a - I_b}{2} \; ; \; I_{CM} = I_a + I_b \quad (3)$$

$$\begin{bmatrix} V_{CM} \\ V_{DM} \end{bmatrix} = \begin{bmatrix} \frac{1}{2} & \frac{1}{2} \\ 1 & -1 \end{bmatrix} \begin{bmatrix} V_a \\ V_b \end{bmatrix}; \begin{bmatrix} I_a \\ I_b \end{bmatrix} = \begin{bmatrix} \frac{1}{2} & 1 \\ \frac{1}{2} & -1 \end{bmatrix} \begin{bmatrix} I_{CM} \\ I_{DM} \end{bmatrix} \quad (4)$$

$$\begin{bmatrix} V_{CM} \\ V_{DM} \end{bmatrix} = [P][I][P^{-1}] \begin{bmatrix} I_{CM} \\ I_{DM} \end{bmatrix} \quad (5)$$

with

$$[P] = \begin{bmatrix} \frac{1}{2} & \frac{1}{2} \\ 1 & -1 \end{bmatrix}$$

$$\begin{bmatrix} V_{CM} \\ V_{DM} \end{bmatrix} = \begin{bmatrix} \frac{Z_{aa} + Z_{ab} + Z_{ba} + Z_{bb}}{4} & \frac{Z_{aa} - Z_{ab} + Z_{ba} - Z_{bb}}{2} \\ \frac{Z_{aa} + Z_{ab} - Z_{ba} - Z_{bb}}{2} & Z_{aa} - Z_{ab} - Z_{ba} + Z_{bb} \end{bmatrix} \begin{bmatrix} I_{CM} \\ I_{DM} \end{bmatrix} \quad (6)$$

$$\begin{bmatrix} V_{CM} \\ V_{DM} \end{bmatrix} = \begin{bmatrix} Z_{CM} & Z'_{conversion} \\ Z_{conversion} & Z_{DM} \end{bmatrix} \begin{bmatrix} I_{CM} \\ I_{DM} \end{bmatrix}. \quad (7)$$

In our specific context, we measure four impedances directly using an impedance analyser while the converter is off and connected to the load. The following steps detail the procedure's progression:

- $Z_{CM}$ is measured between the two short-circuited lines on one side and the ground on the other side.
- $Z_{DM}$ is measured between line **a** and line **b** while isolating the earth.

- $Z_{aa}$ is measured between line a and earth,
- $Z_{bb}$ is measured between line b and earth.

The resulting curves are then obtained as shown in Figure 5.

From these measurements, it is observed that the impedances $Z_{CM}$, $Z_{aa}$, and $Z_{bb}$ are identical.

The equality between $Z_{aa}$, $Z_{bb}$, and $Z_{CM}$ is based on the symmetry of the Buck converter design, ensuring a uniform distribution of impedances between each line and ground. In theory, $Z_{aa}$ and $Z_{bb}$ should be equal, and the common-mode impedance $Z_{CM}$ should match them, reflecting the converter's optimal electromagnetic balance. Impedance measurements confirm this, showing that $Z_{aa}$, $Z_{bb}$, and $Z_{CM}$ are nearly identical across the frequency range tested. While real-world factors may introduce slight variations, they are negligible and do not significantly affect the model's performance. Thus, the assumption $Z_{aa} = Z_{bb} = Z_{CM}$ remains valid for evaluating and optimizing the converter's electromagnetic behavior.

This allows us to propose a symmetrical electrical impedance model as shown in Figure 6. The envisioned model consists of two parallel RLC circuits, positioned between each line and the ground. Similarly, the impedance $Z_{DM}$ is represented using two parallel RLC circuits positioned between lines a and b.

Starting from the diagram in Figure 6, we can calculate the impedance $Z_{aa}$ , $Z_{bb}$ , $Z_{CM}$ , and $Z_{DM}$ . These theoretical impedances can be compared to the measured impedances $Z'_{aa}$, $Z'_{bb}$ $Z'_{CM}$ and $Z'_{DM}$ in the same configuration. The comparisons between measured and calculated curves are presented in Figure 7.

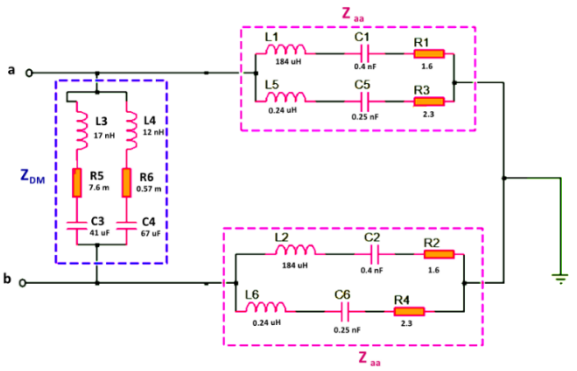


Figure 6. EMC Impedance Model of the Converter.

## 4. STABILITY OF ZMC AND ZMD IMPEDANCES AT OPERATING POINTS

The study of $Z_{CM}$ and $Z_{DM}$ impedance stability in a Buck converter uses a black-box approach, which is essential for analyzing the system's behavior without requiring detailed circuit knowledge. This approach is critical for electromagnetic compatibility and EMI filter design, as stable impedances at different operating points help minimize electromagnetic interference.

However, traditional measurement instruments face challenges under high-power conditions. Specifically, network and impedance analysers struggle with transients, causing unstable data acquisition. Despite these challenges, $Z_{CM}$ and $Z_{DM}$ remain stable across a wide load range (10 % to 80 %), with

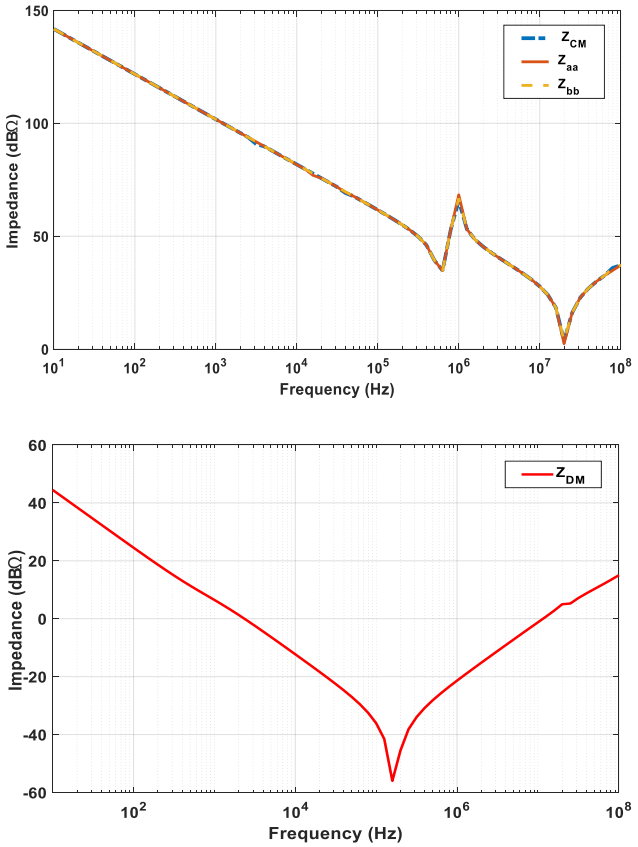


Figure 5. Impedance measured in dBΩ.

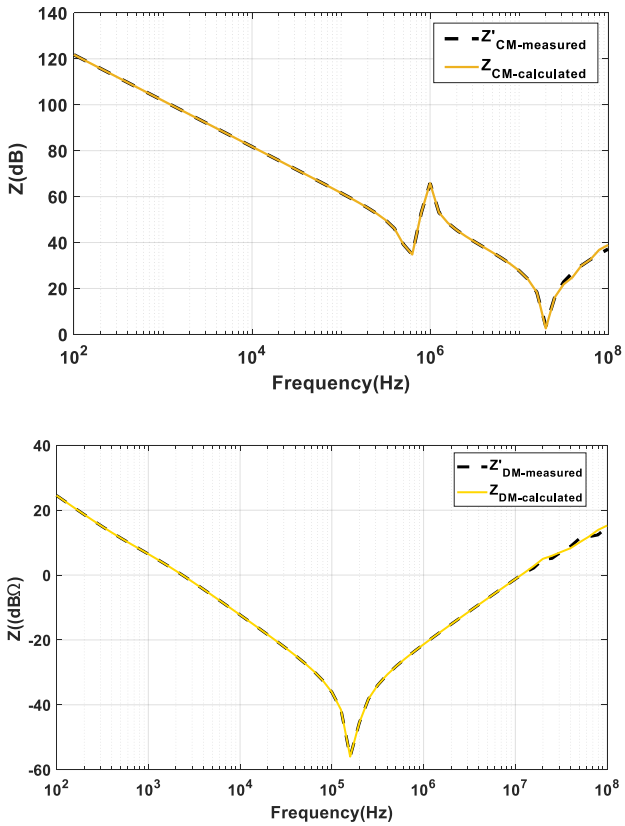


Figure 7. Simulation - measurement comparison.

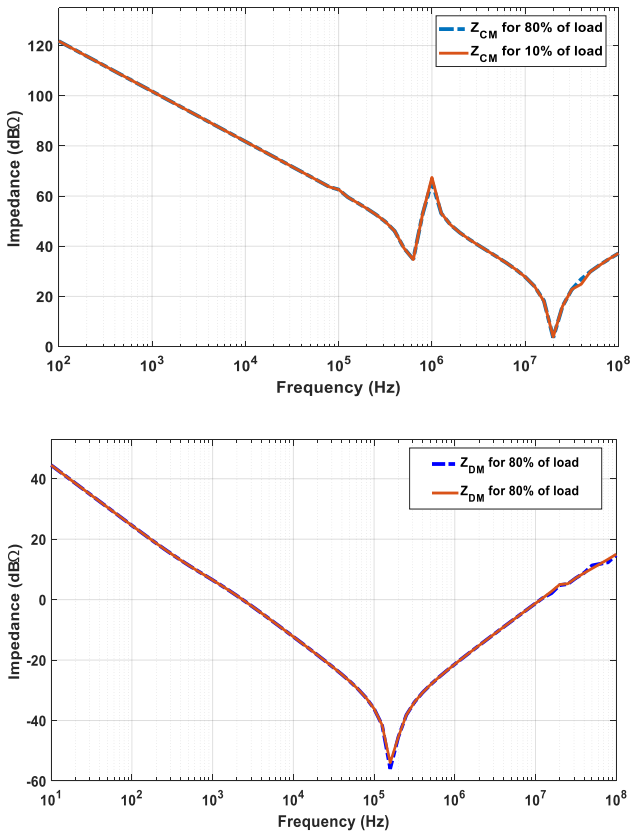


Figure 8. Stability of $Z_{CM}$ and $Z_{DM}$ Impedances as a Function of Applied Load.

the values measured at rest closely matching those observed under dynamic conditions.

As shown in Figure 8, $Z_{CM}$ and $Z_{DM}$ remain constant within the 10 % to 80 % load range, which supports the validity of static modelling for moderate loads. However, beyond 80 % load, a slight decrease in $Z_{DM}$ is observed, likely due to parasitic inductances. Therefore, incorporating a dynamic Line Impedance Stabilization Network would offer a more realistic assessment of impedance under variable loads.

It is also important to note that impedance measurements were taken at rest to avoid complications arising from switching frequency and parasitic effects at high loads, which could distort results.

In conclusion, the results confirm the stability of $Z_{CM}$ and $Z_{DM}$ in the studied ranges, thereby justifying the use of static models for EMI filter design. Consequently, despite the challenges inherent in measurement techniques, the study provides reliable insights for practical applications in EMC and EMI mitigation.

## 5. EXTRACTION OF THE $V_{CM}$ AND $I_{DM}$ SOURCES

The EMC model needs to be complemented with equivalent sources for common mode and differential mode. The mode conversion phenomena will be limited due to the symmetry of the impedances, simplifying the extraction of sources. To identify these sources, the converter is powered through two identical Line Impedance Stabilization Networks, positioned on each line between the system under test and the network. Figure 9 depicts the corresponding equivalent EMC model for this measurement configuration.

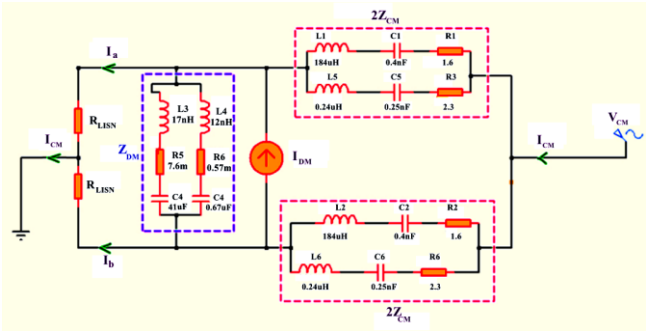


Figure 9. Equivalent Model of the Test Circuit.

Starting from the complete EMC model in Figure 9, we can calculate the disturbance sources $V_{CM}$ and $I_{DM}$ using the following equations (8), (9):

$$I_a + I_b = I_{CM} \Rightarrow V_{CM} = (I_a + I_b)\left(\frac{Z_{lisn} + 2\,Z_{CM}}{2}\right) \quad (8)$$

$$I_a - I_b = 2\frac{\frac{4\,Z_{CM}\,Z_{DM}}{4\,Z_{CM}+Z_{DM}}\,I_{DM}}{2\,Z_{lisn} + \frac{4\,Z_{CM}\,Z_{DM}}{4\,Z_{CM}+Z_{DM}}} \quad (9)$$

$$I_{DM} = (I_a - I_b)\left(\frac{Z_{lisn}}{4\,Z_{CM}} + \frac{Z_{lisn}}{Z_{DM}} + \frac{1}{2}\right). \quad (10)$$

After identifying the impedances, the disturbance sources can be determined by calculating the sum and difference of the currents at the converter input, denoted as "$I_a + I_b$" and "$I_a - I_b$". Before simulating these currents, it is crucial to establish a comprehensive "black-box" model of the LISNs. This model enables accurate impedance characterization of the LISNs [26], [27], which is performed as close as possible to the housing units to ensure precision. For this characterization, a 50 Ω termination is added in parallel with the 1 kΩ resistance within the LISN, as depicted in Figure 10.

The LISN is essential for measuring conducted noise in EMC. It provides a stable 50 Ω impedance between the equipment under test and the power network, thereby isolating noise for accurate measurements. Composed of inductors and capacitors, it acts as a low-pass filter, blocking high frequencies while allowing the passage of the power current.

Here is the schematic showing the LISN and its output impedance, which illustrates the stability of the impedance at 50 Ω.

The CISPR 16-1-2 standard allows a tolerance of ±20 % on the output impedance due to component variations and parasitic effects. However, the LISN remains much more accurate than measurements without it, where the network impedance would be unknown. Within the 150 kHz to 30 MHz range, the LISN's impedance is designed to be stable and close to 50 Ω, ensuring reproducible measurements that comply with CISPR standards.

Indeed, the separation of common-mode and differential-mode noise is essential for analysing conducted electromagnetic emissions (EMC). In this context, common-mode noise refers to the noise that is present simultaneously on both conductors (phase and neutral) with respect to ground, whereas differential-mode noise represents the noise between the conductors. Thus, two main methods are used to measure these types of noise: current probes and isolation transformers.

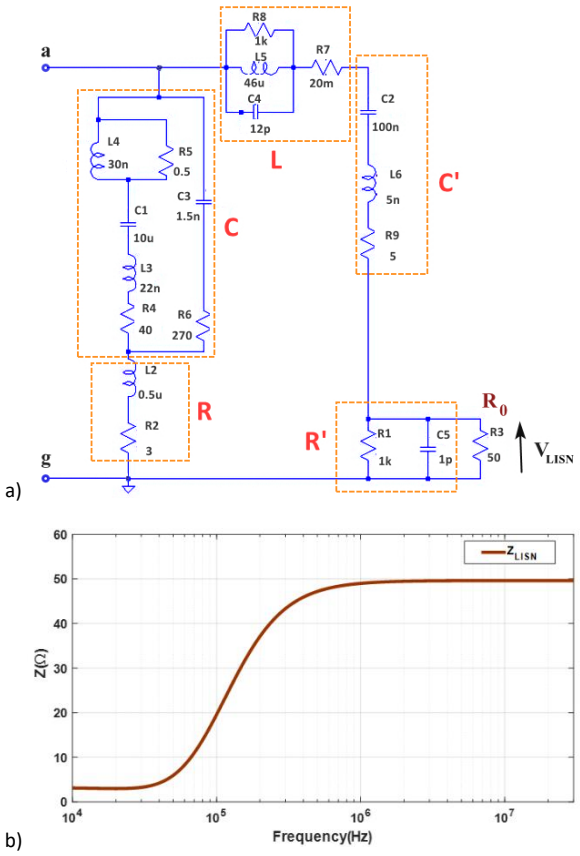


Figure 10. Conducted EMI measurement via a) the real LISN and b) its Equivalent Impedance.

To determine VCM and IDM, simulations were conducted to obtain $I_a + I_b$ and $I_a - I_b$ at a specific operating point. These simulated current values provided the basis for calculating the spectra of the common-mode and differential-mode sources.

This is a diagram showing a current probe measuring the phase and neutral currents, depicted in Figure 11. As a result, the current probe allows for the calculation of CM (the sum of the currents) and DM (the difference between the currents). However, this method, while simple, requires high-quality probes to avoid errors caused by parasitic impedances.

This is a diagram illustrating an isolation transformer with its inputs and outputs, as shown in Figure 12. In contrast, isolation transformers use broadband transformers to add or subtract the phase and neutral signals. Modern versions, such as transmission-line transformers, offer excellent performance up to 30 MHz while minimizing parasitic effects.

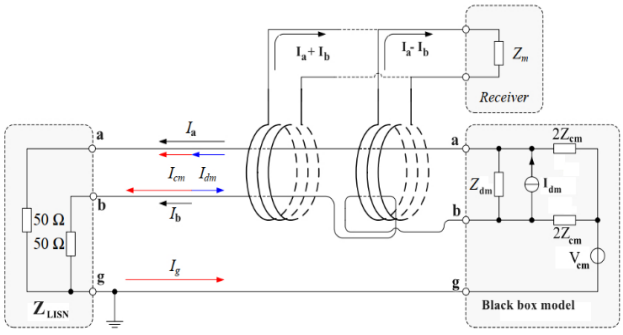


Figure 11. Measurement of CM and DM with a Current Probe.

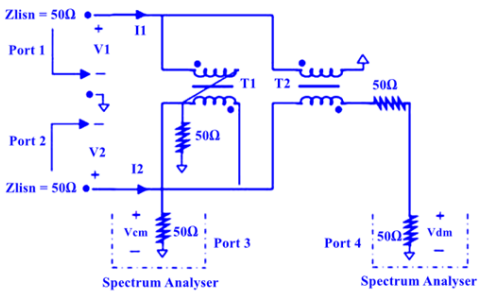


Figure 12. Isolation Transformer for CM and DM Modes.

Furthermore, the spectral components of the CM and DM currents were then derived using equations (8) and (9), as illustrated in Figure 13. This approach enables a detailed analysis of the CM and DM behaviour in the system under the defined operating conditions.

The representation of the common-mode voltage and the differential-mode current provides a better understanding of conducted disturbances. VCM is particularly sensitive to parasitic voltages between the lines and ground, as well as capacitive and inductive couplings, leading to a higher background noise. This phenomenon is further amplified by system asymmetries, which make the common mode more vulnerable to external disturbances. In contrast, IDM, associated with the circulating currents between the lines and more effectively controlled by the converter's design, is less impacted by such interferences. This distinction confirms the validity of the black-box model, which integrates these equivalent sources for accurate modelling and optimal EMC filtering.

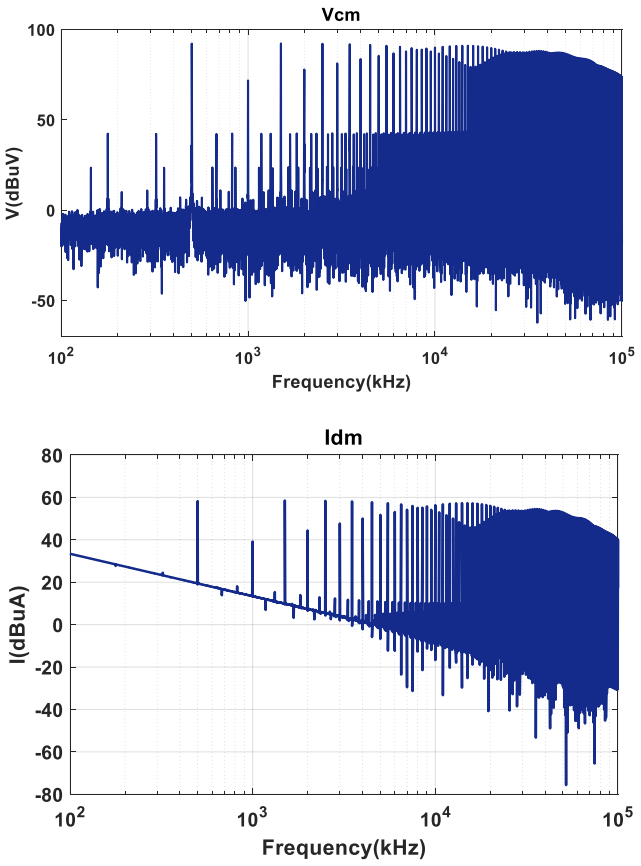


Figure 13. Calculated spectrum of CM and DM sources.

## 6. VALIDATION OF THE MODEL

The studied system is a Buck converter designed to minimize parasitic effects and ensure wiring symmetry. The common-mode and differential-mode impedances were accurately modelled, incorporating parasitic inductances and distributed capacitances of the PCB, valid up to 30 MHz The LISN was also modelled in detail, including parasitic effects and non-linearities, validated through measurements. The method, adaptable to real-world systems, allows for parameter adjustments in complex wiring configurations. A sensitivity analysis confirms the model's robustness against minor variations, enhancing its practical applicability for precise EMC measurements.

To verify that the proposed EMC model can accurately represent the levels of generated electromagnetic disturbances, we reconstructed the voltages across the resistances (50 Ω) of the LISNs using the model presented in Figure 14. At the same time, these voltages were directly measured across the resistances of each LISN.

This EMC model integrates the disturbance sources and characteristic impedances of the system, thereby enabling precise simulation and prediction of the electromagnetic behaviour of the converter. Based on this modelling, it is possible to optimally design two distinct filtering structures: a common mode filter and a differential mode filter.

The validation of this model relies on the comparison between the measured noise spectra and the simulated spectra, as shown in Figure 14. This comparison reveals a good match in the VLISN voltage values between the experimental results and the calculated ones. This agreement confirms the accuracy of the EMC model and validates the methodology used to predict conducted emissions in the system.

## 7. CONCLUSION

The systematic approach presented for characterizing the DC-DC converter (buck converter) employed in the energy management and charging systems of electric vehicles facilitates the construction of an accurate behavioural model in the frequency domain, specifically adapted to the typical DC network configuration within these vehicles. This model captures the intricate interactions between various vehicle components, such as the battery, electric motors, and electronic control systems, with a particular emphasis on minimizing electromagnetic emissions to ensure optimal system performance and compliance with EMC standards. In contrast to other works that focus on the challenges associated with the size of EMI filters or automotive application optimization, this study concentrates on the identification of an equivalent circuit model, which functions as a black-box representation of the system under test. This methodology significantly reduces the computational time required for simulations without compromising model accuracy, thereby enabling the efficient optimization of EMC filter design. The application of model compression techniques is of paramount importance in complex simulations, particularly within the context of automotive applications, where both simulation speed and accuracy are critical for the effective optimization of system designs and the reduction of electromagnetic interference.

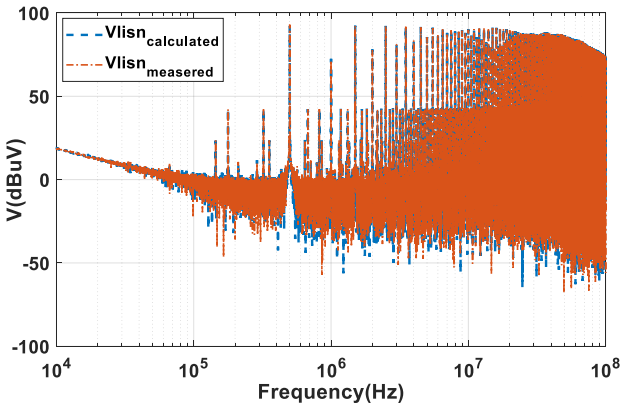


Figure 14. Measured and calculated spectra of voltage across the resistance of each LISN.

## REFERENCES


[1] K. M. Muttaqi, M. E. Haque, Electromagnetic Interference Generated from Fast Switching Power Electronic Devices International Journal of Innovations in Energy Systems and Power, Vol. 3, no. 1 (April 2008).

[2] Z. M'barki, A. A. Salih, Y. Mejdoub, K. S. Rhazi, Digital pseudo-random modulation: a key to EMI reduction in EVS boost converters, Int. Journal of Applied Power Engineering (IJAPE), vol. 13, no. 3, Sep. 2024, p. 594.
DOI: 10.11591/ijape.v13.i3.pp594-602

[3] L. Zhe, D. Pommerenke, EMI specifics of synchronous DC-DC buck converters, 2005 Int. Symp. on Electromagnetic Compatibility, EMC 2005, Chicago, IL, USA, 8-12 August 2005, vol. 3, pp. 711-714.
DOI: 10.1109/ISEMC.2005.1513616

[4] Y. Yinghua, G. Honglin, W. Xinhua, T. Jinfei, Study on Soft Switching Technology to Reduce Electromagnetic Interference of PWM Inverter, Energy Procedia, vol. 17, 12/31, 2012, pp. 384–390.
DOI: 10.1016/j.egypro.2012.02.110

[5] K.-R. Li, K.-Y. See, R. M. Sooriya Bandara, Impact Analysis of Conducted Emission Measurement Without LISN, IEEE Transactions on Electromagnetic Compatibility, vol. 58, no. 3, Jun. 2016, pp. 776–783.
DOI: 10.1109/temc.2016.2533539

[6] A. Ali, J. Chuanwen, M. Khan, S. Habib, Y. Ali, Performance evaluation of ZVS/ZCS high efficiency AC/DC converter for high power applications, Bulletin of the Polish Academy of Sciences Technical Sciences, vol. 68, 01/01 2020, pp. 793-807.
DOI: 10.24425/bpasts.2020.134185

[7] Y. Chuang, High-Efficiency ZCS Buck Converter for Rechargeable Batteries, IEEE Transactions on Industrial Electronics, vol. 57, no. 7, 2010, pp. 2463-2472.
DOI: 10.1109/TIE.2009.2035459

[8] Z. M'barki, Y. Mejdoub, K. Senhaji Rhazi, Implementing Pseudo-Random Control in Boost Converter: An Effective Approach for Mitigating Conducted Electromagnetic Emissions, Indonesian Journal of Electrical Engineering and Informatics (IJEEI), vol. 11, 03/17. 2023.
DOI: 10.52549/ijeei.v11i3.4832

[9] Z. M'barki, K. S. Rhazi, Y. Mejdoub, Practical Implementation of Pseudo-random Control in Step-Down Choppers and Its Efficiency in Mitigating Conducted Electromagnetic Emissions, in Artificial Intelligence and Smart Environment, Cham, Y. Farhaoui, A. Rocha, Z. Brahmia, and B. Bhushab, Eds., 2023, Springer International Publishing, pp. 674-682.

[10] A. Farhadi, A. Jalilian, Modeling and Simulation of Electromagnetic Conducted Emission Due to Power Electronics Converters, 2006 Int. Conf. on Power Electronic, Drives and Energy Systems, New Delhi, India, 12-15 December 2006, pp. 1-6.
DOI: 10.1109/PEDES.2006.344331

[11] M. Laour, R. Tahmi, C. Vollaire, Modeling and Analysis of Conducted and Radiated Emissions Due to Common Mode

Current of a Buck Converter, IEEE Transactions on Electromagnetic Compatibility, vol. 59, no. 4, 2017, pp. 1260-1267.
DOI: 10.1109/TEMC.2017.2651984

[12] L. Wan, A. H. Beshir, X. Wu, X. Liu, F. Grassi, G. Spadacini, Black-box Modeling of Converters in Renewable Energy Systems for EMC Assessment: Overview and Discussion of Available Models, Chinese Journal of Electrical Engineering, vol. 8, no. 2, 2022, pp. 13-28.
DOI: 10.23919/CJEE.2022.000011

[13] C. Rostamzadeh, Synchronous rectified step-down converter susceptibility to conducted and radiated EMI, 2008 IEEE Int. Symp. on Electromagnetic Compatibility, Detroit, MI, USA, 18-22 August 2008, pp. 1-5.
DOI: 10.1109/ISEMC.2008.4652080

[14] B. Nassireddine, B. Abdelber, C. Nawel, D. Abdelkader, B. Soufyane, Conducted EMI Prediction in DC/DC Converter Using Frequency Domain Approach, Int. Conf. on Electrical Sciences and Technologies in Maghreb (CISTEM), Algiers, Algeria, 28-31 October 2018, pp. 1-6.
DOI: 10.1109/CISTEM.2018.8613398

[15] A. Ait Salih, Z. M'barki, Y. Mejdoub, K. Senhaji Rhazi, Electromagnetic Modeling in 'Black Box' Mode of a DC-DC Power Converter (BUCK), Proc. of the Int. Conf. on Connected Objects and Artificial Intelligence (COCIA2024), Casablanca, Morocco, 8-10 May 2024, pp. 199–205.
DOI: 10.1007/978-3-031-70411-6_31

[16] M. Amara, C. Vollaire, M. Ali, F. Costa, Black Box EMC Modeling of a Three Phase Inverter, 2018 Int. Symp. on Electromagnetic Compatibility (EMC EUROPE), Amsterdam, The Netherlands, 27-30 August 2018, pp. 642–647.
DOI: 10.1109/emceurope.2018.8485007

[17] J. Rocha, M. Santos, J. Costa, Voltage Spikes in Integrated CMOS Buck DC-DC Converters: Analysis for Resonant and Hard Switching Topologies, Procedia Technology, vol. 17, 11/24, 2014.
DOI: 10.1016/j.protcy.2014.10.243

[18] N. Shinde, S. Sankad, S. L. Patil, Design and Study Voltage Characteristics of Buck Converter by Matlab Simulink, 2nd Int. Conf. on Trends in Electronics and Informatics (ICOEI), Tirunelveli, India, 11-12 May 2018, pp. 680-683.
DOI: 10.1109/ICOEI.2018.8553695

[19] L. Wan, A. Beshir, X. Wu, X. Liu, F. Grassi, G. Spadacini, Assessment of Validity Conditions for Black-Box EMI Modelling of DC/DC Converters, 2021 IEEE International Joint EMC/SI/PI and EMC Europe Symposium, Raleigh, NC, USA, 26 July-13 August 2021, pp. 581-585.
DOI: 10.1109/EMC/SI/PI/EMCEurope52599.2021.9559274

[20] L. Fang Lin, Y. Hong, Investigation of EMI, EMS and EMC in power DC/DC converters, The Fifth Int. Conf. on Power Electronics and Drive Systems, vol. 1, 2003, pp. 572-577.

[21] Z. M'barki, A. Ait Salih, Y. Mejdoub, K. Senhaji Rhazi, Enhancing Conducted EMI Mitigation in Boost Converters: A Comparative Study of ZVS and ZCS Techniques, in Artificial Intelligence, Data Science and Applications, Cham, Y. Farhaoui, A. Hussain, T. Saba, H. Taherdoost, and A. Verma, Eds., 2024, Springer Nature Switzerland, pp. 434-441.

[22] Z. M'Barki, A. Ait Salih, Y. Mejdoub, K. Rhazi, Strategic electromagnetic interferences suppression in boost converters: zero-switch techniques, Int. Journal of Advances in Applied Sciences, vol. 13, 04/03 2024, pp. 340-350.
DOI: 10.11591/ijaas.v13.i2.pp340-350

[23] M. Pashaei, M. Hasanisadi, F. Tahami, Comprehensive Conducted Emission Analysis of the Three-Phase and Single-Phase LLC Resonant Converters for EV Application, IEEE Transactions on Electromagnetic Compatibility, vol. 65, no. 5, Oct. 2023, pp. 1556–1564.
DOI: 10.1109/temc.2023.3280362

[24] J. Bačmaga, A. Barić, Modeling of Conducted EM Emissions of Synchronous Buck Converters for Different Voltage Conversion Ratios, IEEE Transactions on Electromagnetic Compatibility, vol. 63, no. 6, 2021, pp. 2124-2133.
DOI: 10.1109/TEMC.2021.3069546

[25] Z. M'barki, K. Rhazi, Optimization of electromagnetic interference conducted in a devolver chopper, Proc. of the 2nd Int. Conf. on Electronic Engineering and Renewable Energy Systems, ICEERE 2020, Saidia, Morocco, 13-15 April 2020, LNEE, vol. 681. Springer, Singapore (2021), pp. 523–529.
DOI: 10.1007/978-981-15-6259-4_55

[26] P. C. Chen, W. C. Lin, M. C. Tsai, G. C. Hsieh, H. I. Hsieh, Analysis, Simulation and Design of Soft-Switching Mechanisms in DC-to-DC Step-Down Converter, IEEE 4th Int. Future Energy Electronics Conf. (IFEEC), Singapore, 25-28 November 2019, pp. 1-5.
DOI: 10.1109/IFEEC47410.2019.9015023

[27] V. Wuti, A. Luangpol, K. Tattiwong, S. Trakuldit, A. Taylim, C. Bunlaksananusorn, Analysis and Design of a Zero-Voltage-Switched (ZVS) Quasi-Resonant Buck Converter Operating in Full-Wave Mode, 6th Int. Conf. on Engineering, Applied Sciences and Technology (ICEAST), Chiang Mai, Thailand, 1-4 July 2020, pp. 1-4.
DOI: 10.1109/ICEAST50382.2020.9165351